SUPPLEMENTARY INFORMATION

Supplementary Figure 1

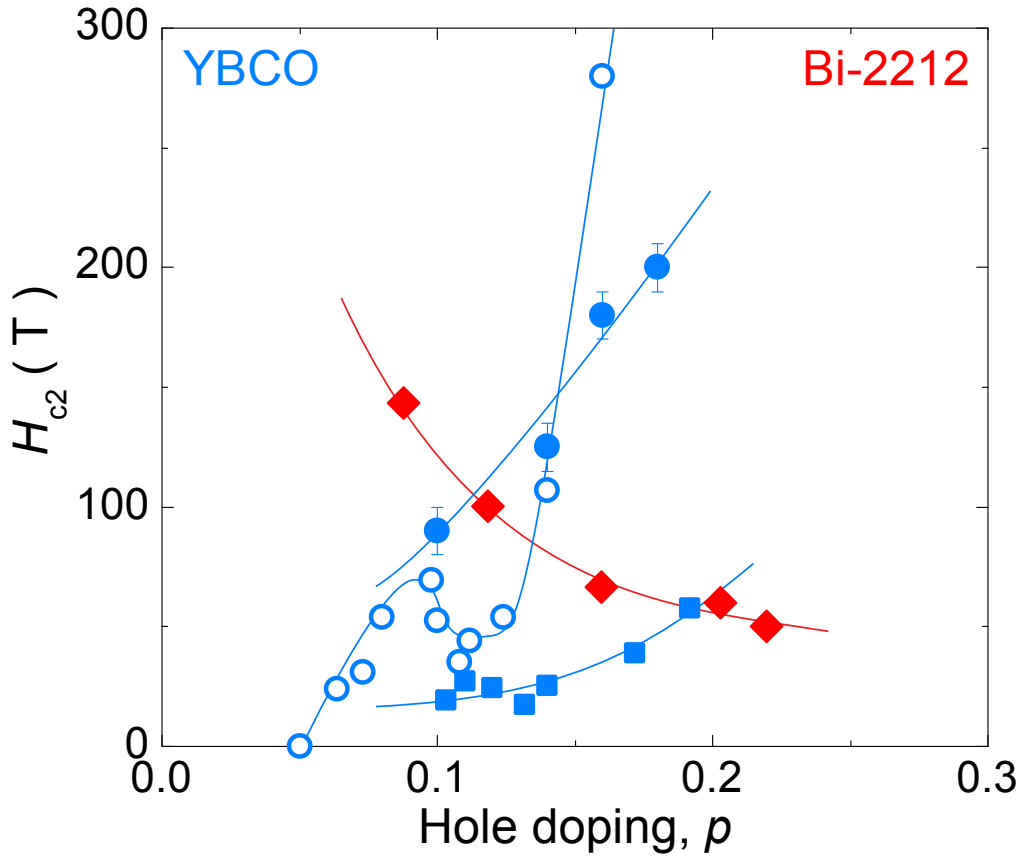

Supplementary Figure 1. Comparing different indirect estimates of H_{c2} in cuprates (see text): 1) from the coherence length extracted from superconducting fluctuations in the conductivity of YBCO above T_c (open blue circles [6]; closed blue circles [41]); 2) from the coherence length extracted from the vortex core size estimated from muon measurements on YBCO in low fields at $T << T_c$ (blue squares [42]); 3) as the field where the Nernst signal vanishes in Bi-2212 (diamonds [2]).

Supplementary Figure 2

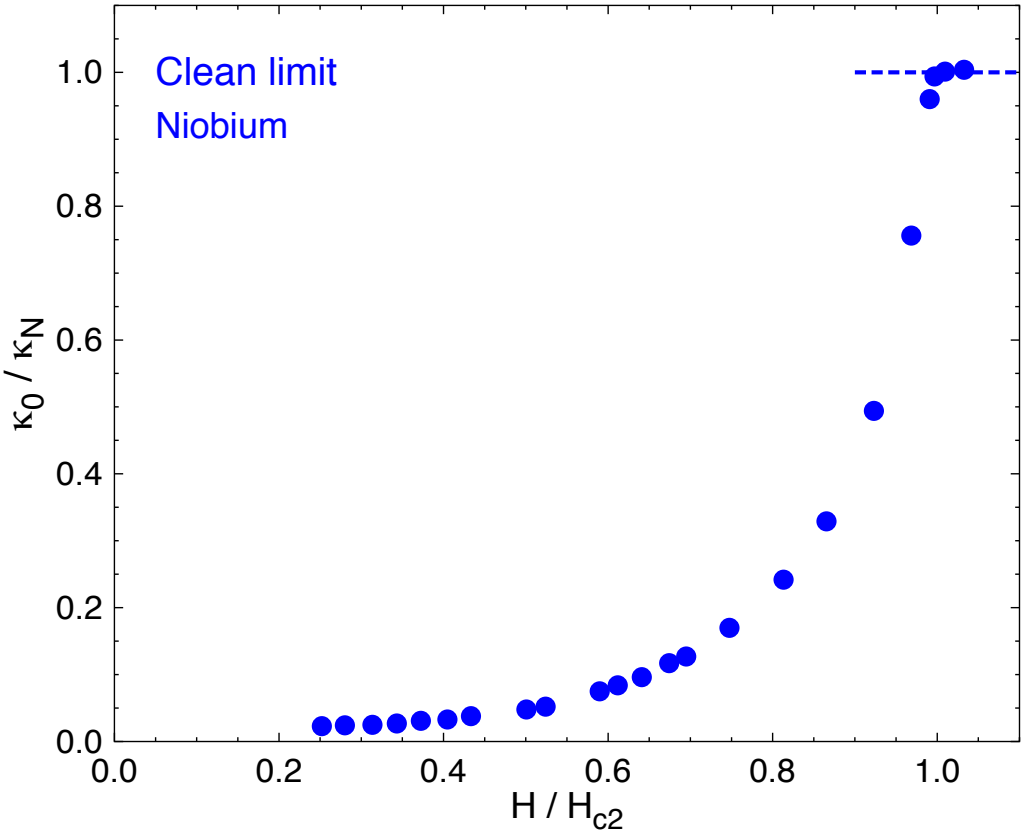

Supplementary Figure 2. Thermal conductivity κ as a function of magnetic field in the limit of $T = 0$, for the *s*-wave superconductor Nb [43], for a sample in the clean limit. With decreasing field, κ shows a sharp drop at H_{c2}, as vortices suddenly introduce an extra scattering mechanism. We use a similar drop to directly determine H_{c2} in clean samples of the cuprate superconductors YBCO and Y124.

Supplementary Figure 3

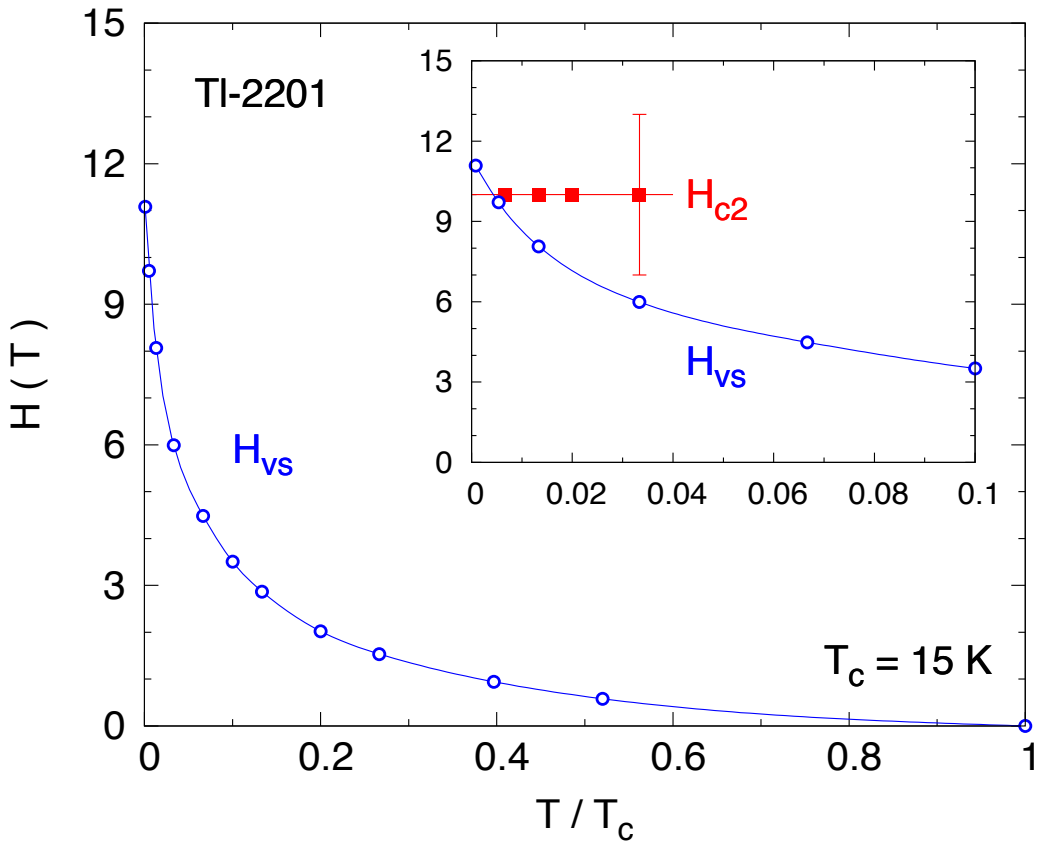

Supplementary Figure 3. *H-T* diagram of strongly overdoped Tl-2201. Temperature dependence of the critical field H_{vs} below which the resistance of Tl-2201 is zero, measured in a highly overdoped sample with T_c = 15 K (open blue circles [44]), and plotted vs T / T_c. Inset: Comparison of $H_{vs}(T)$ (open blue circles) with $H_{c2}(T)$ obtained from thermal conductivity on a sample with T_c = 15 K (red squares, from Supplementary Figure 4), at low temperature. We see that within error bars, H_{vs} = H_{c2} in the T = 0 limit. We also see that $H_{vs}(T)$ drops rapidly with increasing temperature, while $H_{c2}(T)$ is independent of temperature initially. All lines are a guide to the eye.

Supplementary Figure 4

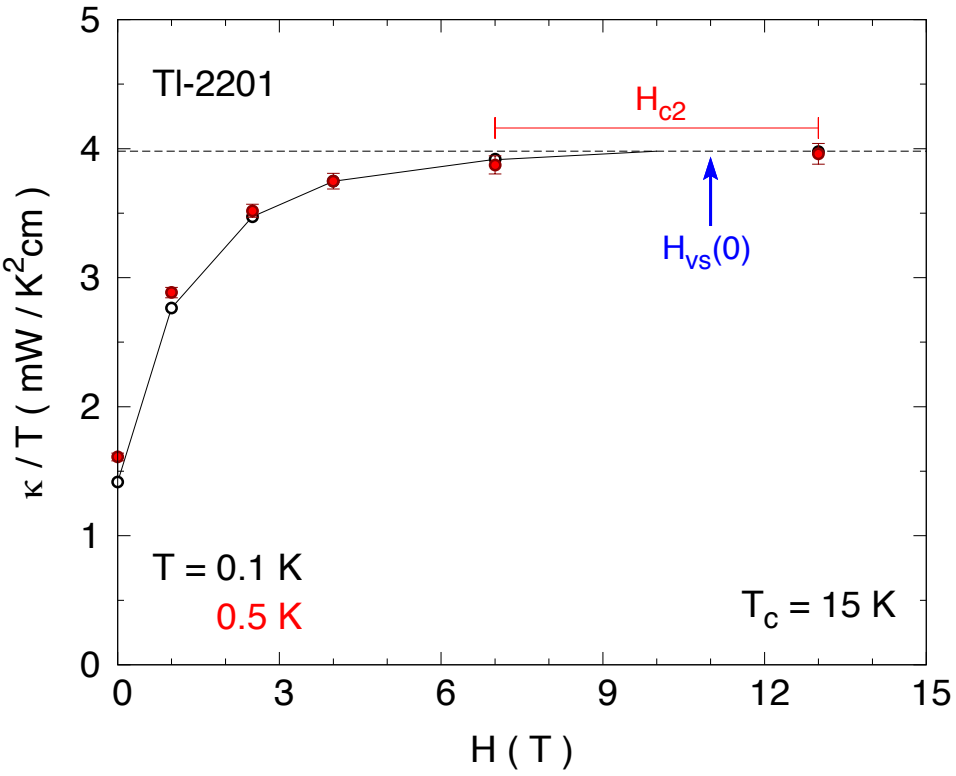

Supplementary Figure 4. Thermal conductivity κ of the *d*-wave cuprate superconductor $Tl_2Ba_2CuO_6$ as a function of magnetic field, at T = 0.1 K (open black circles) and T = 0.5 K (full red circles), for a highly overdoped (T_c = 15 K) sample in the dirty limit (Γ = 0.5 Γ_c , l_0 ~ ξ_0 [45]). H_{c2} is identified here as the field above which κ / T saturates (range shown in red). The blue arrow marks the value of $H_{vs}(0)$ (see Supplementary Figure 3).

Supplementary Figure 5

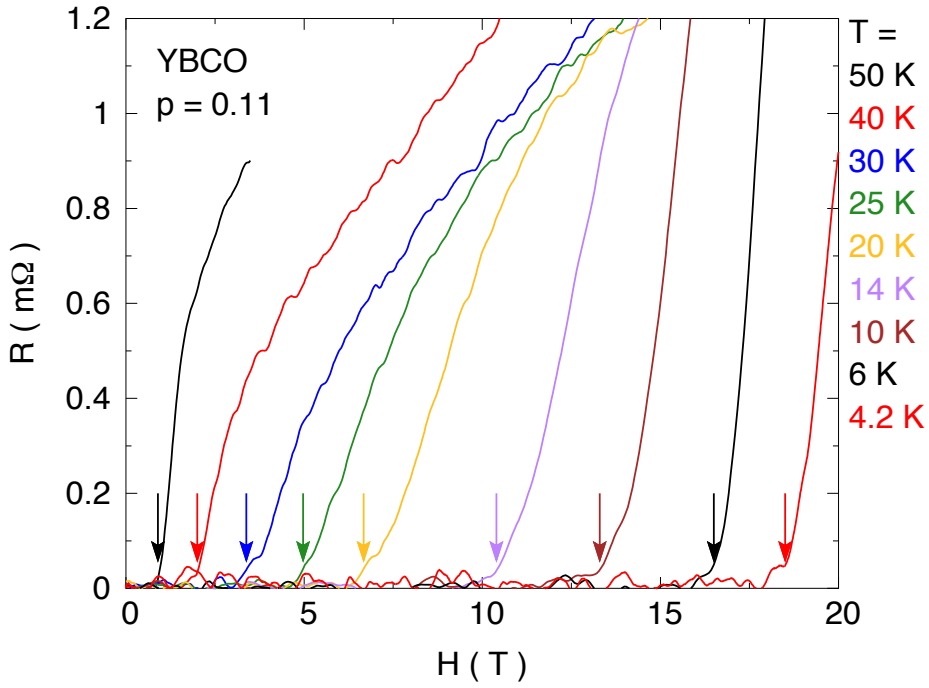

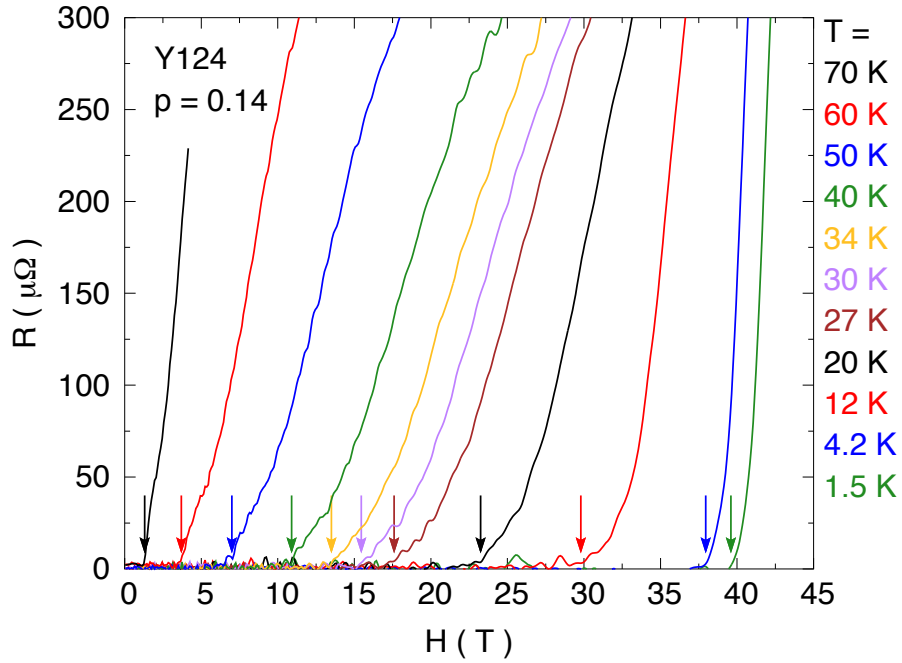

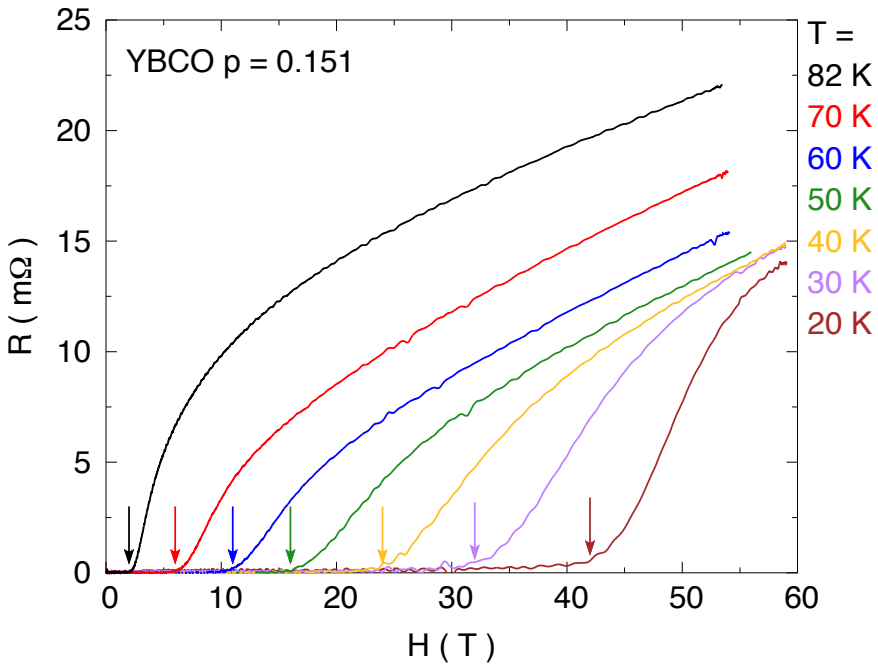
YBCO p = 0.151
T =
82 K
70 K
60 K
50 K
40 K
30 K
20 K
R (mΩ)
H (T)
0
5
10
15
20
25
0
10
20
30
40
50
60

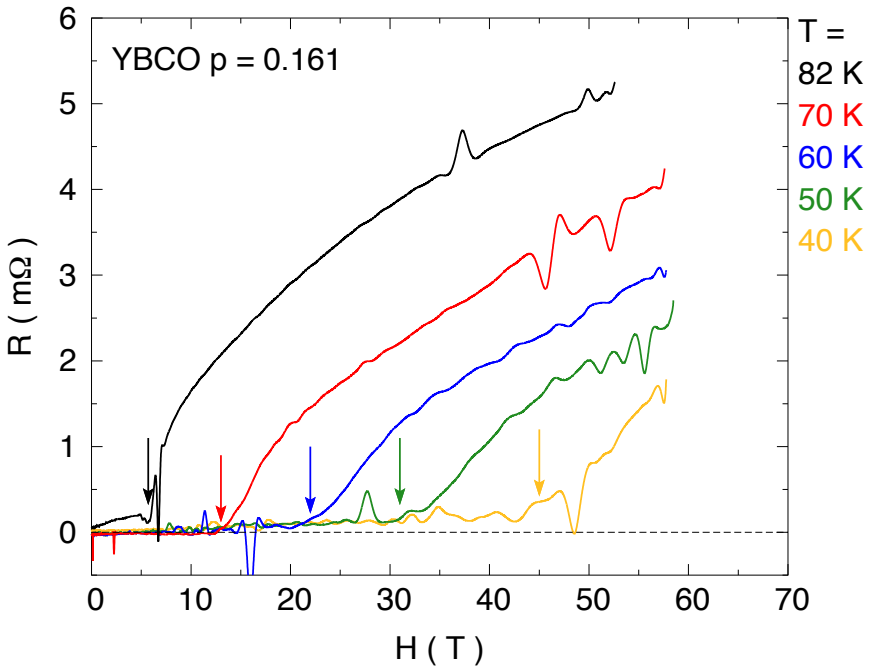
YBCO p = 0.161
T =
82 K
70 K
60 K
50 K
40 K
R (mΩ)
H (T)
0
1
2
3
4
5
6
0
10
20
30
40
50
60
70

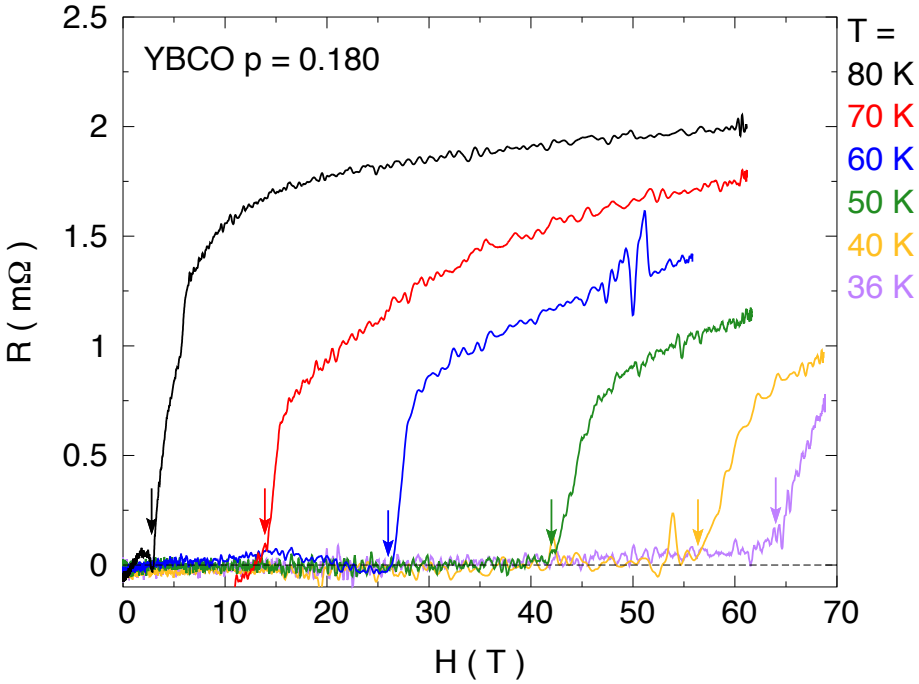
YBCO p = 0.180
T =
80 K
70 K
60 K
50 K
40 K
36 K
R (mΩ)
H (T)
0
0.5
1
1.5
2
2.5
0
10
20
30
40
50
60
70

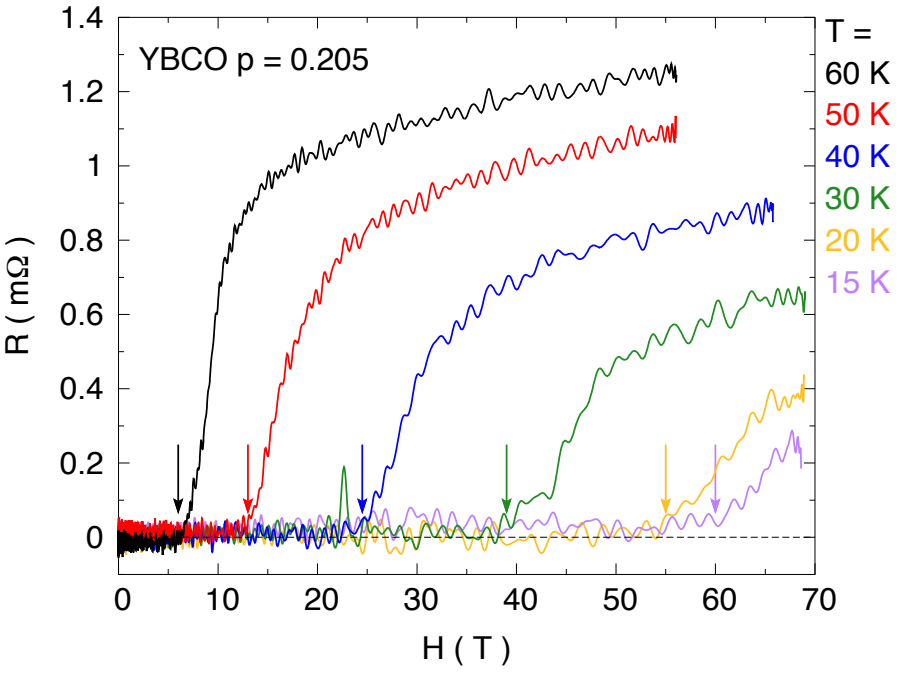
YBCO p = 0.205
T =
60 K
50 K
40 K
30 K
20 K
15 K
R (mΩ)
H (T)
0
0.2
0.4
0.6
0.8
1
1.2
1.4
0
10
20
30
40
50
60
70

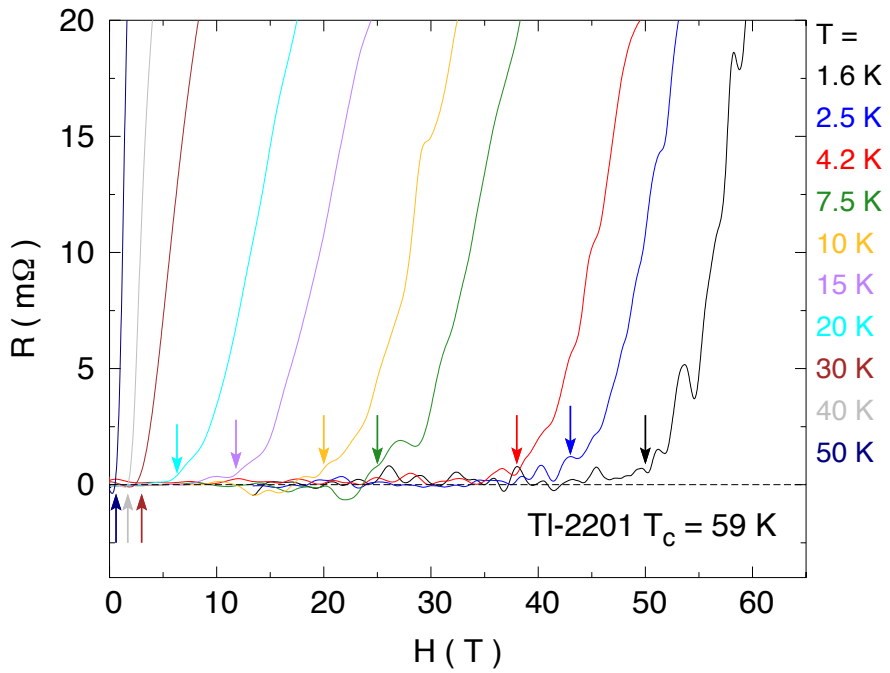

Supplementary Figure 5. (7 panels above). In-plane electrical resistance *R* of YBCO, Y124 and Tl-2201 as a function of magnetic field *H* at different temperatures, as indicated, for various dopings *p*, as indicated in each panel. The data for Y124 (*p* = 0.14) are from ref. 11. The onset of the vortex-solid phase is at the field H_{vs} below which *R* = 0. In practice, H_{vs} is the start of the rapid rise in *R* vs *H* (arrows), above the noise (and in some cases above a small offset). The values of H_{vs} vs *T* are plotted in Supplementary Figure 6 and Fig. 3.

Supplementary Figure 6

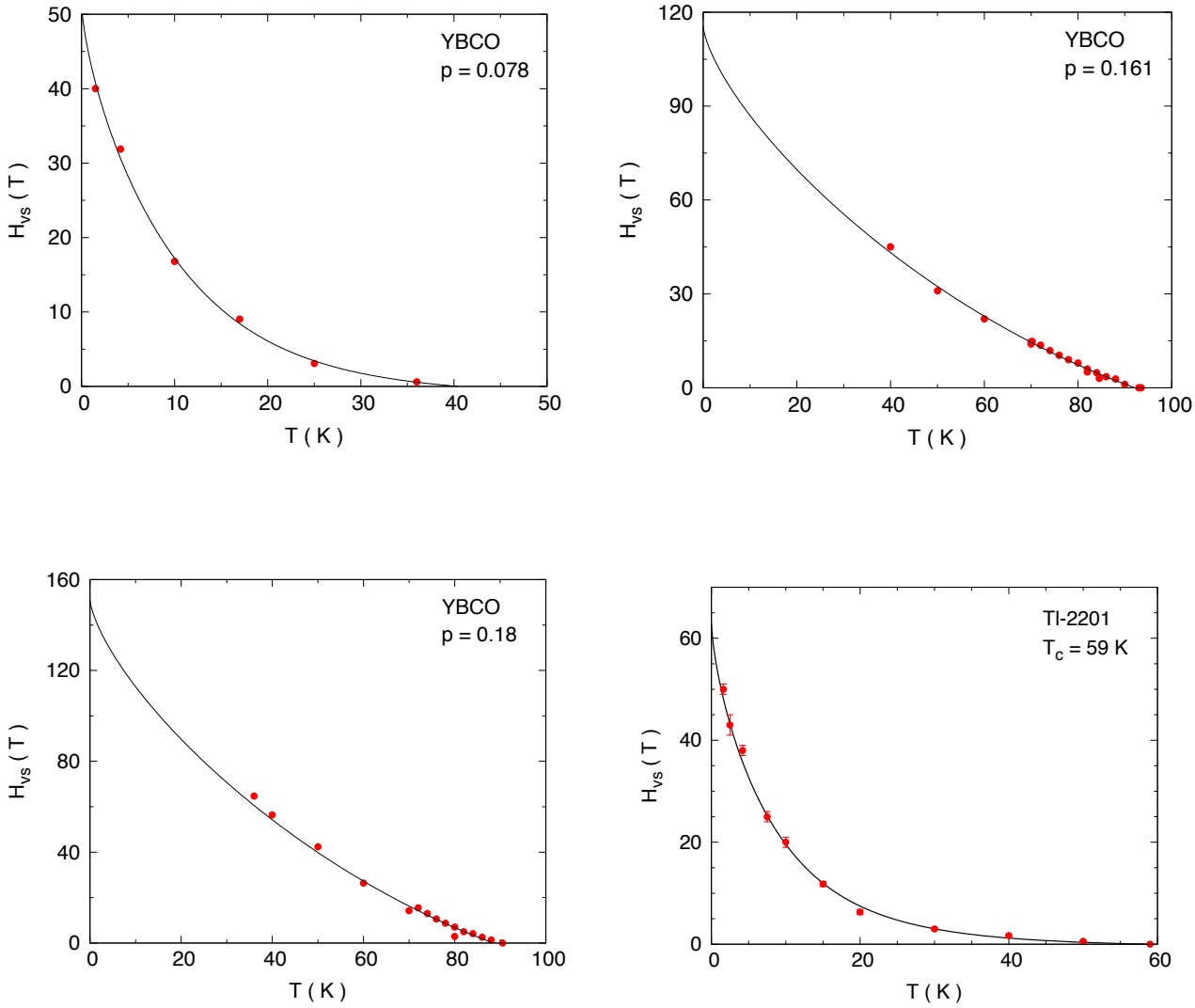

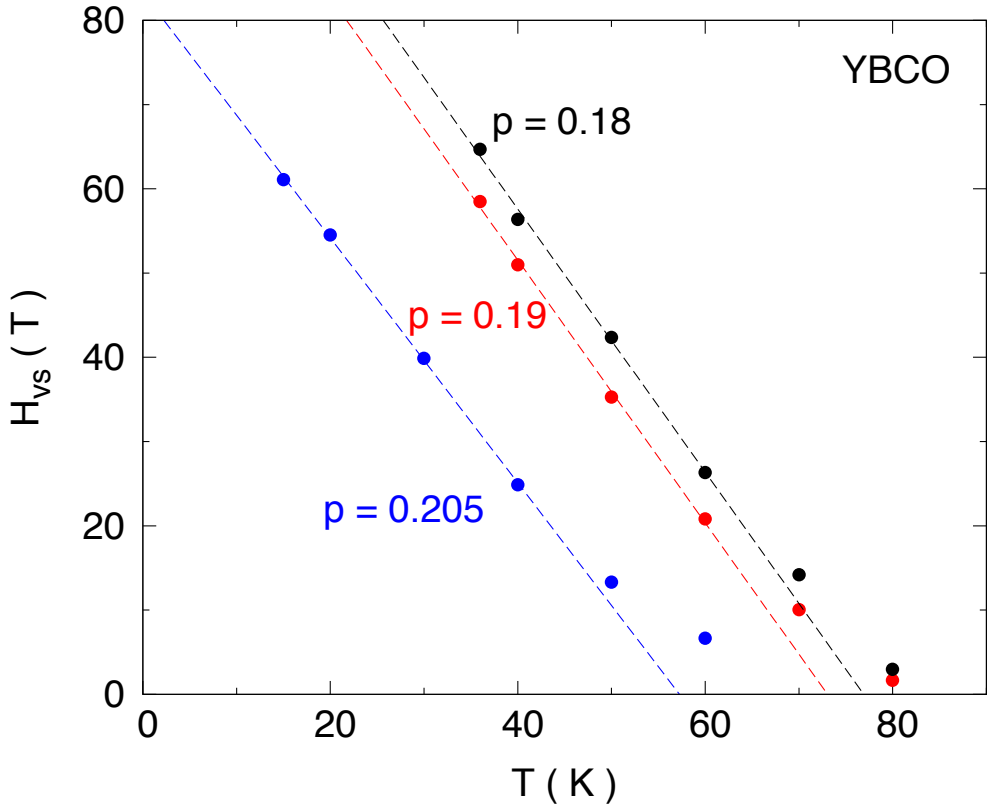

Supplementary Figure 6. (5 panels above). Temperature dependence of the critical field H_{vs} below which the resistance is zero, measured by electrical resistivity in several samples of YBCO and Tl-2201 (from Supplementary Figure 5), with doping p as indicated in each panel (see also Fig. 2d and Fig. 3). The solid line is a fit of the data to the theory of vortex-lattice melting [1] (as performed in ref. 14), from which we extrapolate the value of H_{vs} at T = 0 : $H_{vs}(T{=}0) = H_{c2}$. In the last panel, we compare the raw data at the highest three dopings in YBCO (p = 0.180, 0.190 and 0.205), showing that $H_{vs}(T)$ is highest, and hence H_{c2} is strongest, at p = 0.180.

Supplementary Figure 7

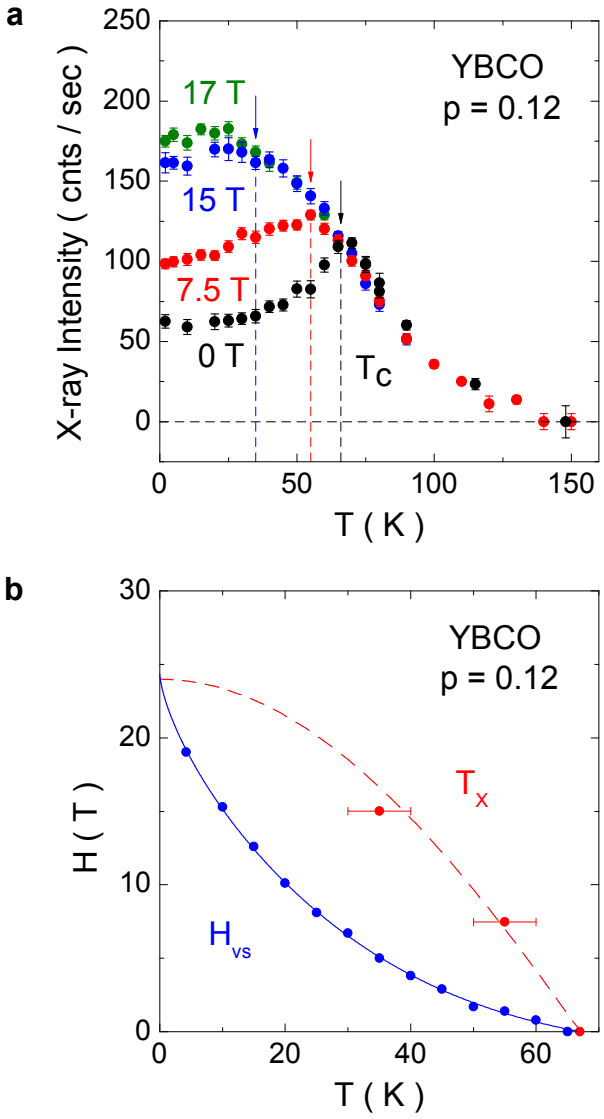

Supplementary Figure 7. Competition between charge order and superconductivity. **a)** Intensity of charge-density-wave modulations in YBCO at p = 0.12 detected by X-ray diffraction, in magnetic fields as indicated [24]. The arrows mark the onset of the competition with superconductivity, at T_X. **b)** H - T diagram comparing the $H_{vs}(T)$ curve for YBCO at p = 0.12 (blue line and data; Fig. 3c) and $T_X(H)$ (red circles, from panel a). The $T_X(H)$ data points are seen to lie well above the $H_{vs}(T)$ boundary. Instead, they track the same $H_{c2}(T)$ curve (dashed line) as our thermal conductivity data at p = 0.11 (Fig. 3a) and p = 0.14 (Fig. 3b).

Supplementary Figure 8

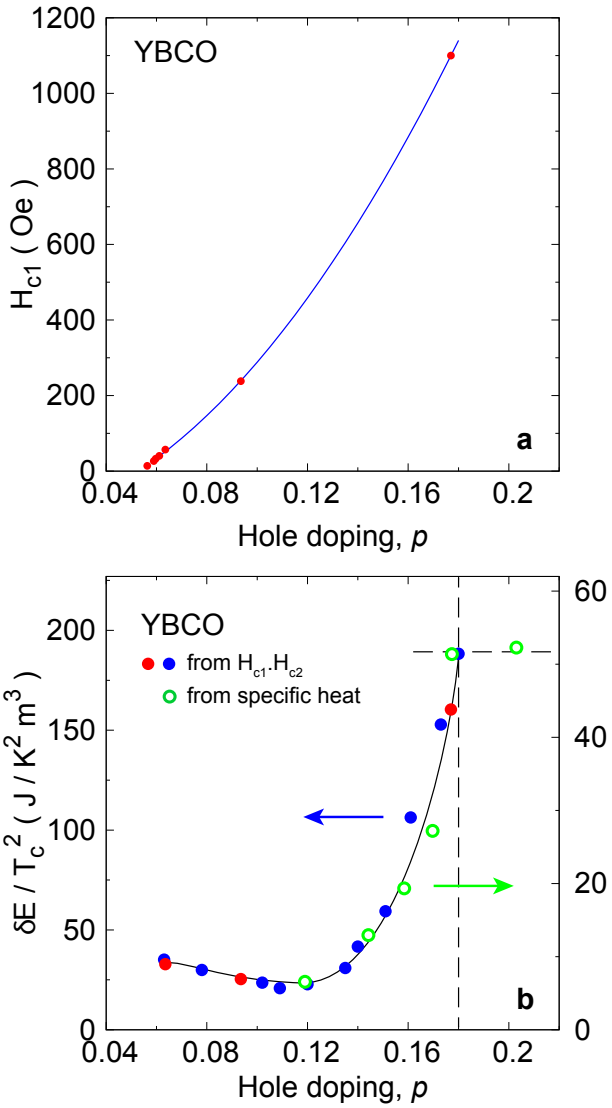

Supplementary Figure 8. a) Lower critical field H_{c1} in YBCO obtained from magnetization measurements [12,27] (full red circles). The blue line is a smooth curve interpolating through the 7 available data points. **b)** Doping dependence of the condensation energy δE in YBCO, plotted as δE / T_c^2 vs p, where δE is calculated from the product of H_{c1} and H_{c2} (full circles, left axis; see Supplementary Note 4). Red circles represent dopings where H_{c1} was actually measured; blue circles correspond to dopings for which H_{c1} was obtained by interpolation (blue line in panel a). Our values of δE are compared with those obtained through an analysis of specific heat data in Ca-doped YBCO (open circles [28]; right axis). Note the 8-fold drop in δE / T_c^2 below p_2 (vertical dashed line), attributed to a corresponding drop in the density of states.

Supplementary Note 1

THERMAL CONDUCTIVITY OF YBCO IN HIGH MAGNETIC FIELDS

Note that κ is the sum of a phonon part (κ_p) and an electronic part (κ_e): $\kappa = \kappa_p + \kappa_e$. Below H_{c2}, an increase in H excites quasiparticles but also enhances vortex scattering, two counteracting effects that leave κ_e relatively flat, until vortex scattering is removed upon approaching H_{c2}. Excited quasiparticles scatter phonons, and this can cause κ_p to decrease with H, depending on the relative importance of other phonon scattering processes. Above H_{c2}, this effect disappears and $\kappa_p(H)$ should be constant. A positive normal-state magneto-resistance will cause κ_e to decrease for $H > H_{c2}$, and possibly also for $H < H_{c2}$. Note that there may be a phononic contribution to the jump in κ at H_{c2}. This would not affect any of our conclusions.

We stress that our observation of a sizable drop in κ below H_{c2} is owed to the fact that ortho-II oxygen-ordered YBCO and stoichiometric Y124 are two underdoped cuprates with exceptionally low levels of disorder, consistent with the observation of quantum oscillations, largest by far in those two particular materials. As seen in Fig. 1a, our data on YBCO display large quantum oscillations above H_{c2}, confirming the high purity of our samples and the high sensitivity of our technique.

Unlike the thermal conductivity, the specific heat of a type-II superconductor is not affected by vortex scattering and so is much less sensitive to the transition out of the vortex state at H_{c2}. In a *d*-wave superconductor, the electronic specific heat will grow approximately as $C_e \sim H^{1/2}$ and saturate above H_{c2}. High-field specific heat data on YBCO at $p = 0.1$ up to $H = 45$ T are consistent with $C_e \sim H^{1/2}$ up to 25 T [5], but cannot currently establish or rule out a saturation above 25 T. Note that in the dirty limit, when the additional scattering from vortices has little impact, κ and C have a similar, rather featureless H dependence (see Figs. 2a and 2b).

Supplementary Note 2

THERMAL CONDUCTIVITY OF TYPE-II SUPERCONDUCTORS

In a type-II superconductor at $T << T_c$, the thermal conductivity above H_{c2} is limited by the elastic mean free path of the electrons in the normal state. As the field is lowered below H_{c2}, the onset of the vortex state, vortices introduce an extra scattering mechanism. If the normal-state mean free path l_0 is much longer than the inter-vortex separation, *i.e*. if $l_0 >> \xi_0$, where ξ_0 is the $T = 0$ coherence length that dictates the value of $H_{c2} = \Phi_0 / 2 \pi \xi_0^2$, then the mean free path will suddenly become much shorter below H_{c2}. As a result of this mechanism, the thermal conductivity of any clean type-II superconductor drops sharply as H crosses below H_{c2}. This drop can therefore be used to determine H_{c2}. As expected, theoretical calculations do obtain such a drop at H_{c2}, whether for *s*-wave [46] or *d*-wave [8, 47] superconductors.

In Supplementary Figure 2, a sharp drop in κ vs H is clearly seen in the clean *s*-wave superconductor Nb, as H falls below H_{c2} [43]. In Fig. 2b, we see that a sharp drop is also observed in a clean sample of the *d*-wave superconductor KFe_2As_2 [9], making an accurate determination of H_{c2} straightforward. This sample has an impurity scattering rate $\Gamma = 0.05\ \Gamma_c$ [9], where Γ_c is the critical scattering rate to suppress T_c to zero. (In a *d*-wave superconductor, $\hbar\Gamma_c = 0.88\ k_B T_c$.) However, in a dirty sample, with $\Gamma = 0.5\ \Gamma_c$ [10], κ rises much more gradually vs H (Fig. 2b), as the specific heat would, and no pronounced anomaly is seen at H_{c2}, making it harder to pinpoint the onset of the vortex state. This comparative study of clean and dirty samples of KFe_2As_2 shows nicely how a long mean free path makes the signature of H_{c2} in κ vs H sharper, and more clearly identifiable.

In Fig. 1e, calculations for a clean *d*-wave superconductor [8, 47] are seen to agree very well with the data on clean KFe_2As_2, over the entire field range.

Supplementary Note 3

WIDTH OF THE RESISTIVE TRANSITION IN Y124 : FROM H_{vs} to H_n

As a function of magnetic field, three factors contribute to the width of the resistive transition from the superconducting state to the normal state. Two intrinsic factors are: 1) the width of the vortex-liquid state, just above $H_{vs}(T)$, where vortices exist but are not pinned; 2) the region of paraconductivity, above $H_{c2}(T)$, where well-defined vortices no longer exist but there are superconducting fluctuations. From electric (or thermo-electric) measurements, it is very difficult to tell where one regime ends and the other begins, making it impossible in practice to pin down $H_{c2}(T)$ from such measurements. The third factor is extrinsic: the resistive transition may be broadened by inhomogeneity in the sample. In YBCO samples, for example, a variation in oxygen content will cause a variation in doping and hence in T_c or H_{vs} across the sample.

By studying Y124, which is stoichiometric and thus much less susceptible to doping inhomogeneity than YBCO, we minimize the extrinsic width. In Fig. 3b, we plot both H_{vs} vs T and H_n vs T for Y124, from resistivity data in ref. 11. H_n is defined as the field below which the resistivity deviates from its normal-state behaviour (see B_n defined in refs. 18 and 26). An example of its definition is shown in Fig. 1f. We see that $H_n(T)$ is much flatter than $H_{vs}(T)$ at low T, and consistent with $H_{c2}(T)$. In fact the entire curve of $H_n(T)$ appears consistent with the extrapolation of $H_{c2}(T)$ measured by thermal conductivity up to higher T. In other words, the width of the resistive transition in Y124 is mostly dictated by the vortex liquid phase, with little extrinsic width and minimal paraconductivity, except just above T_c at low H (Fig. 3b).

In summary, although H_n is ill-defined, being dependent on a loose criterion for "deviation" from a model-dependent assumption about the normal-state behavior, and is susceptible to both extrinsic (inhomogeneity) and intrinsic effects (paraconductivity), we find that in Y124, the most homogeneous of cuprates, $H_n(T)$ does match the $H_{c2}(T)$ line that is identified directly and unambiguously from our thermal conductivity data.

Note that by contrast to Y124, where the width of the resistive transition ($H_n - H_{vs}$) decreases in the $T = 0$ limit, down to the lowest T (Supplementary Figure 5), the corresponding width in YBCO starts to increase when T gets below a certain temperature: ~ 10 K for $p = 0.10$ [26], ~ 5 K for

p = 0.11 (Supplementary Figure 5), ~ 20 K for p = 0.12 [18]. We attribute these increasing widths at low T to slight inhomogeneities in doping, unavoidable in even the most ordered YBCO.

Supplementary Note 4

H_{vs} AND H_{c2} IN A STRONGLY OVERDOPED CUPRATE

In Fig. 2, we have benchmarked our findings on underdoped YBCO and Y124 against similar measurements on the overdoped cuprate Tl-2201. Fig. 2a shows that YBCO and Tl-2201 have the expected clean-limit and dirty-limit behaviours, as observed in KFe_2As_2 (Fig. 2b). In Tl-2201, the onset of the more gradual fall in κ with decreasing H yields values of H_{c2} vs T that vary weakly with T at low T, as in YBCO. Fig. 2d shows that the $H_{c2}(T)$ curve extrapolates to a $H_{c2}(0)$ value consistent with the $H_{vs}(0)$ value extrapolated from the resistive $H_{vs}(T)$ curve, again as in YBCO.

Our findings on Tl-2201 with T_c = 33 K are consistent with earlier measurements on Tl-2201 with T_c = 15 K, limited to low temperatures. In Supplementary Figure 3, we plot $H_{vs}(T)$ vs T / T_c for a highly overdoped sample of Tl-2201, with T_c = 15 K, from data in ref. 44. In the T = 0 limit, the data yield $H_{vs}(0)$ = 11 T. Because of the stronger 2D character, $H_{vs}(T)$ drops with increasing T much more rapidly than in YBCO or Y124. An increase to T = 0.5 K (= T_c / 30) is enough to reduce H_{vs} by half of its value at $H_{vs}(0)$ (see inset of Supplementary Figure 3).

In Supplementary Figure 4, we plot κ / T vs H for overdoped Tl-2201, measured on a sample with the same T_c (doping) and residual resistivity (impurity scattering) as that of ref. 44 (from data in ref. 45). These Tl-2201 samples are in the dirty limit, with Γ = 0.5 Γ_c [45], and the curve of κ vs H is indeed very similar to that of dirty KFe_2As_2 with Γ = 0.5 Γ_c (Fig. 2b). There is no sharp anomaly at H_{c2}, but one can still define roughly the field above which κ vs H saturates, giving H_{c2} = 10 ± 3 T. The combined thermal and electrical data show that $H_{c2}(0) = H_{vs}(0)$ in Tl-2201, confirming in an overdoped cuprate our findings in two underdoped cuprates.

Supplementary Note 5

CONDENSATION ENERGY IN YBCO

Having obtained the full curve of H_{c2} vs p (Fig. 4a), we can compute the condensation energy δE of YBCO by using existing data for the lower critical field H_{c1} [12,27], via the standard formula $\delta E = H_c^2 / 2\mu_0$, with $H_c^2 = H_{c1} H_{c2} / (\ln \kappa_{GL} + 0.5)$, using $\kappa_{GL} = 50$, the essentially doping-independent Ginzburg-Landau parameter (ratio of penetration depth to coherence length). To produce a full curve from $p = 0.05$ to $p = 0.18$, we interpolate the H_{c1} data points (Supplementary Figure 8a). The resulting curve for δE is shown in Supplementary Figure 8b, plotted as $\delta E / T_c^2$ vs p.

We can compare our $\delta E(p)$ data for YBCO obtained directly from experiment, without assumptions or model, with an earlier estimate obtained from an analysis of specific heat data on Ca-doped YBCO [28]. This analysis required an estimate of the large phonon background and a model for the normal-state specific heat. (It also used Ca-doped samples, whose higher disorder could affect the magnitude of $\delta E / T_c^2$.) In Supplementary Figure 8b, we see that this analysis is in good qualitative agreement with our data. (Quantitatively, the values of $\delta E / T_c^2$ obtained in ref. 28 appear to be a factor ~ 3-4 smaller than our values.) Both approaches reveal a huge 10-fold drop in $\delta E / T_c^2$ when YBCO goes from $p = 0.18$ to $p = 0.11$. This dramatic drop coincides approximately with the critical doping where Fermi-surface reconstruction takes place [18].

Supplementary Discussion

PRIOR ESTIMATES OF H_{c2}

A clear transition at the upper critical field H_{c2} of a cuprate superconductor has not been reported before. The thermal conductivity in ultraclean YBCO appears to be the first measured property to exhibit a sharp transition at H_{c2}.

The resistive transition at $H_{vs}(T)$ has of course been measured by many groups [*e.g.* 14,18,26]. In YBCO, it has been noted that as a function of doping H_{vs} exhibits a minimum near $p = 0.12$ [14,18]. But it has not until now been known how this critical field and its minimum relate to the real H_{c2}.

Until now, H_{c2} has only been estimated indirectly, using various models and assumptions. In some studies, the superconducting Nernst signal was tracked to high field and H_{c2} was defined as the field where the signal extrapolates to zero [2], yielding H_{c2} values such as displayed in Supplementary Figure 1 (for Bi-2212; red diamonds). This procedure has recently been criticized [7]. Another approach is to extract the contribution of superconducting fluctuations to the electrical conductivity above T_c, making assumptions about the normal-state conductivity, and fit that contribution to Gaussian theory to obtain the $T = 0$ coherence length ξ_0. Then, using the standard expression $H_{c2} = \Phi_0 / 2 \pi \xi_0^2$, one arrives at an estimate of H_{c2}. Two groups have done this for YBCO [6, 41], and their findings are plotted in Supplementary Figure 1 (circles). A third approach is to extract the vortex core size from muon spin relaxation measurements at low H and low T, and equate that with ξ_0. In YBCO, this led to the values of H_{c2} displayed in Supplementary Figure 1 (squares) [42].

These different estimates show a variation by one order of magnitude at any given doping.

Supplementary Methods

MEASUREMENTS OF THE CRITICAL FIELD H_{vs}

In a *H*-*T* diagram, the vortex-solid phase is defined as the region where electrical resistance is zero. In the panels of Supplementary Figure 5, we show raw isotherms of the in-plane electrical resistance as a function of the magnetic field *H* in YBCO, Y124 and Tl-2201, at various dopings. Data such as these are used to determine the onset of the vortex-solid phase of zero resistance at $H_{vs}(T)$, plotted as H_{vs} vs *T* in the various panels of Supplementary Figure 6. Fits to the theory of vortex-lattice melting [1] are performed as in ref. 14, to obtain H_{vs} in the $T = 0$ limit. We equate this $H_{vs}(0)$ with $H_{c2}(0)$ (labeled H_{c2}) for all dopings, as specifically demonstrated for YBCO at $p = 0.11$ (Fig. 3a), Y124 at $p = 0.14$ (Fig. 3b), and Tl-2201 at $p = 0.25$ (Fig. 2d) and $p = 0.26$ (Supplementary Figure 3). The resulting H_{c2} values are listed in Table 1 and plotted in Fig. 4a.

Supplementary References

[41] Rullier-Albenque, F. *et al.* High-field studies of superconducting fluctuations in cuprates: Evidence for a small gap distinct from the large pseudogap. *Phys. Rev. B* **84**, 014522 (2011).

[42] Sonier, J. E. *et al.* Hole-doping dependence of the magnetic penetration depth and vortex core size in $YBa_2Cu_3O_y$.: evidence for stripe correlations near 1/8 hole doping. *Phys. Rev. B* **76**, 134518 (2007).

[43] Lowell, J. & Sousa, J. B. Mixed-state thermal conductivity of type-II superconductors. *J. Low Temp. Phys.* **3**, 65-87 (1970).

[44] Mackenzie, A.P. *et al.* Resistive upper critical field of $Tl_2Ba_2CuO_6$ at low temperatures and high magnetic fields. *Phys. Rev. Lett.* **71**, 1238-1241 (1993).

[45] Proust, C. *et al.* Heat transport in a strongly overdoped cuprate : Fermi liquid and a pure *d*-wave BCS superconductor. *Phys. Rev. Lett.* **89**, 147003 (2002).

[46] Houghton, A. & Maki, K. Thermal conductivity and ultrasonic attenuation in clean type-II superconductors. *Phys. Rev. B* **4**, 843-847 (1971).

[47] Vekhter, I. & Houghton, A. Quasiparticle thermal conductivity in the vortex state of high-T_c cuprates. *Phys. Rev. Lett.* **83**, 4626-4629 (1999).